Geometrical-optics code for computing the optical properties of large dielectric spheres

Xiaobing Zhou, Shusun Li, and Knut Stamnes

Absorption of electromagnetic radiation by absorptive dielectric spheres such as snow grains in the near-infrared part of the solar spectrum cannot be neglected when radiative properties of snow are computed. Thus a new, to our knowledge, geometrical-optics code is developed to compute scattering and absorption cross sections of large dielectric particles of arbitrary complex refractive index. The number of internal reflections and transmissions are truncated on the basis of the ratio of the irradiance incident at the nth interface to the irradiance incident at the first interface for a specific optical ray. Thus the truncation number is a function of the angle of incidence. Phase functions for both near- and far-field absorption and scattering of electromagnetic radiation are calculated directly at any desired scattering angle by using a hybrid algorithm based on the bisection and Newton–Raphson methods. With these methods a large sphere's absorption and scattering properties of light can be calculated for any wavelength from the ultraviolet to the microwave regions. Assuming that large snow meltclusters (1-cm order), observed ubiquitously in the snow cover during summer, can be characterized as spheres, one may compute absorption and scattering efficiencies and the scattering phase function on the basis of this geometrical-optics method. A geometrical-optics method for sphere (GOMsphere) code is developed and tested against Wiscombe's Mie scattering code (MIE0) and a Monte Carlo code for a range of size parameters. GOMsphere can be combined with MIE0 to calculate the single-scattering properties of dielectric spheres of any size. © 2003 Optical Society of America

OCIS codes: 080.2720, 290.5850, 120.0280, 010.2940, 160.4760.

1. Introduction

To model the reflectance of a random medium such as a snow cover or a desert soil surface by using radiative transfer theory, we need basic optical properties (the single-scattering albedo and the phase function or the asymmetry factor) of the individual dielectric particles of which the surface is composed. For small spherical particles such as droplets in water clouds, the optical properties can be computed exactly from Mie theory[1,2] and parameterized as a function of a liquid-water path and droplet size.[3] For non-spherical particles, unlike the spherical case, for which the exact Mie theory is available, no benchmarked computational techniques are generally available, although research on light scattering by nonspherical particles is being actively pursued.[4–8] Grains in wet or liquid-saturated snow [liquid-water content, ≥7%] tend to be cohesionless spherical particles.[9] Thus single-scattering properties of snow grains can be obtained by using Mie scattering theory.[1,2,10,11] However, for moist or low-liquid-content (<7%) snow, grains tend to form multigrain clusters. Clusters of grains are widely observed in snow covers.[12–14] Owing to frequent melt–refreezing cycles, summer snow cover on Antarctic sea ice is characterized by ubiquitous snow meltclusters with grain size of 1-cm order,[15–17] along with ice lenses, ice layers, and percolation columns. Centimeter-scale icy nodules in snow were also observed in winter, after a surface thaw–freeze event.[14,18] It has been found that the albedo is correlated with snow-composite grain size of 1-cm order instead of the single grains of 1-mm order that make up composite grains.[19] This indicates that composite grains such as meltclusters may play an important role in the radiative proper-

X. Zhou (xzhou@nmt.edu) is with the Department of Earth and Environmental Science, New Mexico Institute of Mining and Technology, 801 Leroy Place, Socorro, New Mexico 87801. S. Li (sli@asf.alaska.edu) is with, and X. Zhou is on leave from, the Geophysical Institute, University of Alaska Fairbanks, P.O. Box 757320, Fairbanks, Alaska 99775-7320. K. Stamnes (kstamnes@stevens-tech.edu) is with the Light and Life Laboratory, Department of Physics and Engineering Physics, Stevens Institute of Technology, Castle Point on Hudson Hoboken, New Jersey 07030.

ties of summer snow cover. Retrieval algorithms based on the comparison between radiance or reflectance data obtained from satellite sensors and those computed by radiative transfer models need the single-scattering properties of the target particles.[20] To understand the interaction of electromagnetic radiation with the dielectric particles and its role in the remote sensing of snow cover and desertification, etc., it is imperative to obtain the single-scattering properties of the dielectric particles.

In principle, the single-scattering properties can be calculated by using Mie theory for spheres of any size. But the Mie solutions are expansions in terms of the size parameter $x = 2\pi a/\lambda$, where a is the radius of spherical particles and λ is the wavelength of the incident radiation. Numerous complex terms are needed to obtain converged solutions for large values of x.[21] For this reason, available Mie codes can be used for $x < 20,000$. For large values of x, the best method is the ray-optics approximation.[10,22] The geometrical-optics method (GOM) has been extensively used in scattering of radiation not only from spherical particles[10] but also by nonspherical particles.[23] Results from a Monte Carlo code based on the GOM show that differences in the simulated radiances between the GOM and the Mie computations decrease as the size parameter increases even when the magnitude of the two phase functions at the scattering angle are almost the same.[23] It has been shown that results from the geometrical-optics approach will converge to those obtained by Mie theory when the size/wavelength ratio becomes sufficiently large.[24]

The purpose of this paper is to develop a new geometrical-optics code [geometrical-optics method for sphere (GOMsphere)] based on the GOM for computing single-scattering properties of large dielectric spheres and to apply it to calculate absorption coefficients, scattering coefficients, and phase functions for both near- and far-field absorption and scattering of electromagnetic radiation by large snow grains, which cannot be obtained by using a publicly available Mie code (MIE0). To accomplish this task, we first derive a truncation formula for the number of interfaces (N) required for accurate ray tracing as a function of the angle of incidence (hereafter called the incidence angle) and the ratio of the energy flux incident at the jth interface (j is an integer) to that incident at the first interface ($j = 1$). The benefits of using a truncation criterion (variable N) that depends on the incidence angle in the calculation of the phase function rather than using a constant N are discussed in Subsection 3.B, along with a backward method developed for calculating the phase function on the basis of the solution of a trigonometric equation.

For applications of the GOM to summer snow cover, the shape of the snowmelt clusters or composite grains are assumed to be spherical for simplicity reasons only. The complex refractive indices $\hat{m}$ of snow and ice for the calculations in this paper are taken primarily from the updated compilation by Warren and collaborators.[25,26] Measurements by Kou *et al.*[27] of the imaginary part of the complex refractive index for polycrystalline ice in the 1.45–2.50-µm region agree well with Warren's compilation. Discrepancies between the two data sets in this spectral region occur mainly near 1.50-, 1.85-, and 2.50-µm, with the largest discrepancy near 1.85 µm. Gaps in the data at ultraviolet wavelengths in the 0.25- to 0.40-µm region were filled by Perovich and Govoni.[28] The temperature dependence of the refractive index of ice for $\lambda < 100$ µm is deemed to be negligible for most temperatures that would be found on Earth.[26] With the spectral complex refractive index available, the spectral dependence of the optical properties of a single snow grain can be calculated by using GOMsphere.

2. Single-Scattering Properties—Geometrical-Optics Formalism

Scattering by a particle is actually the sum of the reflection and refraction plus the Fraunhofer diffraction. Reflection and refraction depend on the optical properties of the particle and act to distribute the outgoing (scattered) light in all directions. The amplitude of the Poynting vector of a plane wave F_λ (it is also called the spectral irradiance or energy flux at wavelength λ) is[29]

$$F_\lambda = \frac{m'}{2Z_0} |\mathbf{E}_0|^2 \exp(-\beta z), \quad (1)$$

where $\beta = 4\pi m''/\lambda$ is the absorption coefficient and $Z_0 = \sqrt{\mu_0/\epsilon_0}$ is the impedance of free space. m' and m'' are the real and imaginary parts of the refractive complex $\hat{m}$. $|\mathbf{E}_0|$ is the amplitude of the electric field. z is the distance traveled by the wave in the direction of propagation.

A. Ray Tracing and Truncation

For a dielectric sphere whose radius is much larger than the wavelength of the incident wave, we adopt the ray-tracing method to calculate the single-scattering properties.[10,11] The incident wave is as-
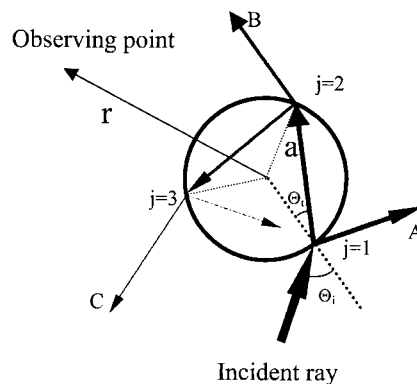

Fig. 1. Ray-tracing diagram. Incident rays will propagate by separation of reflection and refraction. The energy contained in each ray decreases rapidly as it propagates. Rays such as A, B, and C, etc., emerging from the scatterer will experience the same process with other scatterers, resulting in multiple scattering. The weight of each arrowed line denotes the energy content contained in the ray.

sumed to be p polarized, where $p = \parallel$ or $\perp$ indicates that the wave is parallel or perpendicularly polarized. Reflection and transmission occur only at an interface between media with different indices of refraction. Figure 1 illustrates the absorption and scattering by a spherical particle in the geometrical-optics picture. The incidence angle Θ_i is defined as the angle between the ray hitting the sphere and the normal at the hitting point. The initial ray separates into reflected and refracted subrays after it hits the particle surface. Energy contained in each ray decreases rapidly as it propagates by reflection and refraction. Here the direction of the refracted light ray determined from the complex refraction angle is defined in the same way as that from a real refraction angle, but the value is the amplitude of the complex angle or the absolute value of the complex angle. Because light originates from outside the sphere, total internal reflections will not happen because the incidence angle for an internal reflection is equal to or smaller than the refraction or reflection angle at the previous interface. The thickness of the arrowed lines in Fig. 1 denotes this debasement of energy in each ray. At the jth interface, which is defined as the order of interface between the particle and the incident light ray, assuming the incident electric field is $E_{p,i}{}^j$, the reflected $(E_{p,r}{}^j)$ and transmitted $(E_{p,t}{}^j)$ electric fields are[19,30]

$$E_{p,r}{}^j = r_p{}^j E_{p,i}{}^j, \qquad E_{p,t}{}^j = t_p{}^j E_{p,i}{}^j, \qquad (2a)$$

with

$$E_{p,i}{}^j = E_{p,i}, \qquad\qquad\qquad j = 1,$$

$$E_{p,i}{}^j = t_p \prod_{l=2}^{j} (r_p{}^l) \exp[-\beta\xi(j-1)/2] E_{p,i}$$

$$= t_p(-r_p)^{j-2} \exp[-\beta\xi(j-1)/2] E_{p,i}, \quad j \geq 2, \qquad (2b)$$

where

$$r_p{}^j = r_p(\Theta_i, \Theta_t, \hat{m}) = r_p,\ t_p{}^j = t_p(\Theta_i, \Theta_t, \hat{m}) = t_p$$
$$\text{if } j = 1, \text{ and}$$
$$r_p{}^j = r_p(\Theta_t, \Theta_i, 1/\hat{m}),\ t_p{}^j = t_p(\Theta_t, \Theta_i, 1/\hat{m}),$$
$$\text{if } j > 1,$$

and ξ is the path length between two consecutive interfaces.

For absorbing and scattering media the reflection coefficients r_p and the transmission coefficients t_p are complex quantities. Following the discussion in Born and Wolf[31] about wave reflection and transmission of metallic films and setting $\hat{m} \cos \Theta_t = u +$

iv, $i = \sqrt{-1}$, we find that r_p and t_p have the forms[19,32]

$$r_\parallel(\Theta_i, \Theta_t, \hat{m})$$
$$= \frac{[(m'^2 - m''^2)\cos \Theta_i - u] + i(2m'm'' \cos \Theta_i - v)}{[(m'^2 - m''^2)\cos \Theta_i + u] + i(2m'm'' \cos \Theta_i + v)},$$

$$t_\parallel(\Theta_i, \Theta_t, \hat{m})$$
$$= \frac{2(m' + im'')\cos \Theta_i}{[(m'^2 - m''^2)\cos \Theta_i + u] + i(2m'm'' \cos \Theta_i + v)},$$
$$(3a)$$

$$r_\perp(\Theta_i, \Theta_t, \hat{m}) = \frac{(\cos \Theta_i - u) - iv}{(\cos \Theta_i + u) + iv},$$

$$t_\perp(\Theta_i, \Theta_t, \hat{m}) = \frac{2 \cos \Theta_i}{(\cos \Theta_i + u) + iv}, \qquad (3b)$$

$$r_p(\Theta_t, \Theta_i, 1/\hat{m}) = -r_p(\Theta_i, \Theta_t, \hat{m}),$$

$$t_p(\Theta_t, \Theta_i, 1/\hat{m}) = \frac{(u + iv)}{\cos \Theta_i} t_p(\Theta_i, \Theta_t, \hat{m}), \quad (3c)$$

with

$$u = \frac{\sqrt{2}}{2} \{[(m'^2 - m''^2 - \sin^2 \Theta_i)^2 + 4m'^2 m''^2]^{1/2}$$
$$+ (m'^2 - m''^2 - \sin^2 \Theta_i)\}^{1/2},$$

$$v = \frac{\sqrt{2}}{2} \{[(m'^2 - m''^2 - \sin^2 \Theta_i)^2 + 4m'^2 m''^2]^{1/2}$$
$$- (m'^2 - m''^2 - \sin^2 \Theta_i)\}^{1/2},$$

where Θ_i is the incidence angle (real) and Θ_t is the refraction angle (complex). For a spherical particle with an arbitrary absorption coefficient, the sum over the number of interfaces should, in principle, extend to infinity. However, on the basis of the strength of the incident electric field at the jth interface, the series can be truncated at some value, for instance, N, at which interface the electric field is so weak compared with the incident field that additional terms can be neglected.

If the truncation is made when the ratio of the irradiance or energy flux at the jth interface to that incident at the first interface ($j = 1$) is equal to some small tolerance number ς, we can obtain the truncation number N required for convergence through combination of Eqs. (1) and (2b) as[19]

$$N(\Theta_i) = \frac{\beta\xi + 2 \ln|t| - 2 \ln R - \ln \varsigma}{\beta\xi - \ln R}, \qquad (4)$$

where $R = |r|^2$,

$$T = \frac{m'[(um' + vm'')^2 + (vm' - um'')^2]^{1/2}}{(m'^2 + m''^2)\cos \Theta_i} |t|^2,$$

in which $t = [0.5(t_\parallel{}^2 + t_\perp{}^2)]^{1/2}$ and $r = [0.5(r_\parallel{}^2 + r_\perp{}^2)]^{1/2}$. Here $r(t)$, which is defined as the ratio of the amplitude of the reflected (transmitted) electric field to

that of the incident electric field, is referred to as the reflection (transmission) coefficient, whereas $R(T)$, which is defined as the ratio of the energy flux of the reflected (transmitted) wave to that of the incident wave, is called reflectance (transmittance). We neglected the term $\ln m'$ in Eq. (4) as it is generally a small number. The dependence of N on the incidence angle for the case of green light at $\lambda = 0.5$ μm is shown in Fig. 2(a) for an ice sphere of radius $a = 1$ cm. Two cases of ς($= 1.0 \times 10^{-16}$ and 1.0×10^{-4}) are also shown in Fig. 2(a) so that the dependence of N on the tolerance number can be seen. N is a function of the incidence angle, radius of the dielectric sphere, and the truncation tolerance. If ς is just 1.0×10^{-4}, the maximum truncation number is approximately 30 for large incidence angles, but, for incidence angles smaller than 70°, $N = 5$ is enough. For higher accuracy calculation (ς $= 1.0 \times 10^{-16}$), the maximum number of N can be over 300 for large incidence angles. For incidence angles smaller than 70°, $N = 20$ is enough. The

same calculation for $\lambda = 2.0$ μm shows that $N = 2$ is enough for all incidence angles. Glantschnig and Chen[33] compared angular scattering diagrams for $\lambda = 0.49$ μm on the basis of the geometrical-optics approximation for $N = 2$ with results from exact Mie calculations. They found that for $\Theta_i \leq 60°$, the agreement is reasonable, whereas, for large angles the geometrical-optics approach does not give good results. From Fig. 2(a) we can see that, for green light, N increases rapidly with increasing incidence angle when it is greater than approximately 80°. This illustrates that the approximation $N = 2$ is not sufficient for the calculation of light scattering by weakly absorbing particles at large incidence angles, but it is for strongly absorbing particles. The dependence of N on wavelength λ is shown in Fig. 2(b) for $\Theta_i = 60°$. For visible light, ice is weakly absorbing, and attenuation is weak so that a much larger number of ray paths is needed, whereas, in the near infrared, ice is strongly absorbing, and only one or two paths are necessary to extinguish the transmitted radiation.

B. Absorption Properties

If the incident radiation is unpolarized, then the total absorbed energy (summed over all ray paths and integrated over the sphere surface for all incidence angles) becomes[11,19]

$$W_{\text{abs}} = 2\pi a^2 F_0 \int_0^1 T(\mu_i) \sum_{j=2}^{N} [R \exp(-\beta\xi)]^{j-2}$$
$$\times [1 - \exp(-\beta\xi)]\mu_i d\mu_i, \tag{5}$$

where

$$T = \frac{1}{2}(T_{\parallel} + T_{\perp}),$$

with

$$T_p = \frac{m'[(um' + vm'')^2 + (vm' - um'')^2]^{1/2}}{(m'^2 + m''^2)\cos\Theta_i}|t_p|^2,$$

$$R = \frac{1}{2}(R_{\parallel} + R_{\perp}),$$

with $R_p = |r_p|^2$,

$$\xi = |2a \cos\Theta_t|$$
$$= \frac{2a}{m'^2 + m''^2}[(um' + vm'')^2 + (vm' - um'')^2]^{1/2}, \tag{6}$$

with $\mu_i = \cos\Theta_i$. The summation over j in Eq. (5) is from 2 to $N = N(\Theta_i)$. From the total energy absorbed and the initial incident irradiance, the absorp-
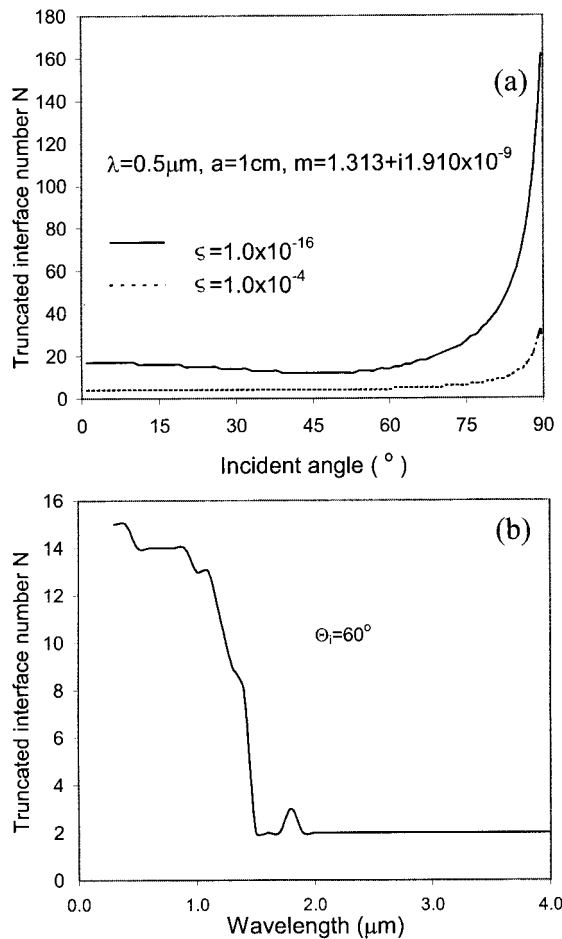

Fig. 2. (a) Maximum number N versus incidence angle for the truncation in the sum series of the calculation of absorption efficiency for an ice sphere with radius $a = 1$ cm and truncation tolerance ς $= 1.0 \times 10^{-16}$ and 1.0×10^{-4} for wavelength $\lambda = 0.5$ μm. (b) The maximum number N versus wavelength λ for the truncation in the sum series of the calculation of absorption efficiency of an ice sphere with radius $a = 1$ cm and truncation tolerance ς $= 1.0 \times 10^{-16}$ for incidence angle $\Theta_i = 60°$.

In figure (a): Truncated interface number N (vertical axis), Incident angle (°) (horizontal axis), $\lambda = 0.5$ μm, $a = 1$ cm, $m = 1.313 + i1.910 \times 10^{-9}$, (a), ς $= 1.0 \times 10^{-16}$, ς $= 1.0 \times 10^{-4}$.

In figure (b): Truncated interface number N (vertical axis), Wavelength (μm) (horizontal axis), (b), $\Theta_i = 60°$.

tion cross section and absorption efficiency are obtained as

$$C_{abs} = \frac{W_{abs}}{F_0} = 2\pi a^2 \int_0^1 T(\mu_i) \sum_{j=2}^N [R\exp(-\beta\xi)]^{j-2}$$

$$\times [1 - \exp(-\beta\xi)]\mu_i d\mu_i$$

$$= 2\pi a^2 \int_0^1 T(\mu_i) \frac{1 - \exp(-\beta\xi)}{1 - R\exp(-\beta\xi)} \mu_i d\mu_i, \quad (7a)$$

$$Q_{abs} = \frac{C_{abs}}{\pi a^2}. \quad (7b)$$

C. Scattering Properties

Within the radiative transfer equation, the phase function is defined as[34,35]

$$P(\tau; \mu, \phi; \mu', \phi') = \frac{4\pi C_{sca}{}^d(\tau; \mu, \phi; \mu', \phi')}{C_{sca}}$$

$$= \frac{4\pi C_{sca}{}^d(\tau, \Theta)}{C_{sca}}, \quad (8)$$

where $\mu = \cos\theta$ and $C_{sca}{}^d$ is the differential scattering cross section. For isotropic media, $C_{sca}{}^d(\tau; \mu, \phi; \mu', \phi')$ depends only on the scattering angle Θ: $\Theta = \arccos[\mu\mu' + \sqrt{1 - \mu^2}\sqrt{1 - \mu'^2}\cos(\phi - \phi')]$. Thus $C_{sca}{}^d(\tau; \mu, \phi; \mu', \phi') = C_{sca}{}^d(\tau, \Theta)$. The physical meaning of $P(\tau; \mu, \phi; \mu', \phi')$ is that it is the probability of a photon scattering from the direction $\Omega' = (\theta', \phi')$ to the direction $\Omega = (\theta, \phi)$. (θ', ϕ') are the polar and azimuth angles prior to scattering, and (θ, ϕ) are those after scattering. The total scattering cross section,

$$C_{sca} = 2\pi \int_0^\pi d\Theta C_{sca}{}^d(\tau, \Theta)\sin\Theta,$$

is the difference between the extinction cross section and the absorption cross section, i.e., $C_{sca} = C_{ext} - C_{abs}$. The phase function is expressed in terms of the scattering cross section and the differential scattering cross section:

$$P(\tau; \mu, \phi; \mu', \phi') = \frac{4\pi C_{sca}{}^d(\tau, \Theta)}{C_{sca}}$$

$$= \frac{2C_{sca}{}^d(\tau, \Theta)}{\int_0^\pi d\Theta C_{sca}{}^d(\tau, \Theta)\sin\Theta}. \quad (9)$$

On the basis of the phase function, the asymmetry factor is defined as

$$g = \langle\cos\Theta\rangle = \frac{1}{4\pi}\int P(\tau; \Theta)\cos\Theta d\Omega$$

$$= \frac{1}{2}\int_{-1}^1 P(\tau; \Theta)\cos\Theta d\cos\Theta. \quad (10)$$

1. Near-Field Scattering

The total energy scattered by a large sphere includes the diffracted, reflected, and transmitted components. Thus the scattering cross section and scattering efficiency of a large sphere can be written respectively as[11]

$$C_{sca} = \frac{\sum_{j=1}^N W_{sca}{}^j}{F_0} = C_{dif} + C_{ref} + C_{tra}, \quad (11a)$$

$$Q_{sca} = \frac{C_{sca}}{\pi a^2}. \quad (11b)$$

Scattered rays at the first interface are exclusively the reflected component. All rays emerging from the second interface on are included in the transmitted component. Using the same procedure that was employed to obtain Eqs. (7), we can derive the second and last components of Eq. (11a) for unpolarized incident radiation as follows:

$$C_{ref} = \frac{W_{sca}{}^1}{F_0} = 2\pi a^2 \int_0^1 R(\mu_i)\mu_i d\mu_i, \quad (12a)$$

$$C_{tra} = \frac{\sum_{j=2}^N W_{sca}{}^j}{F_0} = \pi a^2 \sum_{j=2}^N \int_0^1 [T_\parallel{}^2(\mu_i)R_\parallel{}^{j-2}(\mu_i)$$

$$+ T_\perp{}^2(\mu_i)R_\perp{}^{j-2}(\mu_i)]\exp[-\beta\xi(j-1)]\mu_i d\mu_i.$$

$$(12b)$$

Equation (12a) has the same form as in the case of a nonabsorbing sphere.[11] For the near field, the diffraction is Fresnel diffraction. Fraunhofer diffraction will occur when the viewing distance $r > a^2/\lambda$.[30] For the incident plane waves, Fresnel diffraction is a near-surface phenomenon. For the calculation of scattering at the surface and far-field scattering, it does not contribute anything. Thus we neglect the Fresnel diffraction in the following discussion.

From scattering theory,[10] the scattered irradiance at a distance r from the scattering center is related to incidence irradiance through the differential scattering cross section $C_p{}^d(j, \Theta_i, \Theta)$ by

$$F_p(j, \Theta_i, \Theta) = \frac{C_p{}^d(j, \Theta_i, \Theta)}{r^2} F_0$$

$$= \frac{a^2|\epsilon_p{}^j|^2 D(j, \Theta_i, \Theta)F_0}{r^2}, \quad (13)$$

where

$$D(j, \Theta_i, \Theta) = \frac{\sin(2\Theta_i)}{4\left|(j-1)\dfrac{\cos\Theta_i}{(u^2+v^2)^{1/2}} - 1\right|\sin\Theta},$$

$$\epsilon_p{}^j = \begin{cases} r_p, & j = 1 \\ \dfrac{(u+iv)}{\cos\Theta_i}(t_p)^2(-r_p)^{j-2}\exp[-\beta\xi(j-1)/2], & j \geq 2 \end{cases}.$$

For unpolarized natural light, the phase function [see Eq. (9)] is thus

$$P(\Theta) = \frac{2\pi}{C_{\text{sca}}} \sum_{j,\Theta_i} \sum_p C_p^d(j, \Theta_i, \Theta), \qquad (14a)$$

with

$$C_{\text{sca}} = \pi a^2 \int_0^\pi \sum_{j,\Theta_i} (|\epsilon_\parallel^j|^2 + |\epsilon_\perp^j|^2) D(j, \Theta_i, \Theta) \sin \Theta d\Theta.$$
$$(14b)$$

The sum $\sum_{j,\Theta_i}$ in Eqs. (14) extends over all sets of (j, Θ_i) that make up a scattered light ray emerging at angle Θ. This guarantees that the irradiances of rays emerging at the same scattering angle for a specific incidence angle but from different interfaces, and those for a specific interface but from different incidence angles, are added up. The extinction cross section is determined by

$$C_{\text{ext}} = C_{\text{sca}} + C_{\text{abs}}. \qquad (15)$$

Equations (7)–(12), (14) and (15) constitute the main equations for near-field scattering by large absorbing particles.

2. Far-Field Scattering

For the far-field scattering, the absorption is the same as expressed in Eqs. (7). The only difference between the far-field and the near-field scattering in the calculation of the scattering cross section is due to Fraunhofer diffraction.[10,33] The total differential scattering cross section due to reflection, transmission, and diffraction is given by

$$C_{\text{sca}}^d(\Theta_i, \Theta) = \frac{1}{2} \sum_{j,\Theta_i} \sum_p C_p^d(j, \Theta_i, \Theta)$$
$$+ \frac{a^2 J_1^2(x \sin \Theta)}{\sin^2 \Theta}. \qquad (16)$$

The phase function is easily obtained if we insert Eq. (16) into Eq. (9). It takes the form

$$P(\Theta_i, \Theta) =$$

$$\frac{2 \sum_{j,\Theta_i} \sum_p |\epsilon_p^j|^2 D(j, \Theta_i, \Theta) + \dfrac{4 J_1^2(x \sin \Theta)}{\sin^2 \Theta}}{1 + \displaystyle\int_0^\pi d\Theta \sin \Theta \sum_{j,\Theta_i} \sum_p (\epsilon_p^j)^2 D(j, \Theta_i, \Theta)}. \qquad (17)$$

3. Single-Scattering Properties—Numerical Computations and Comparisons

On the basis of the formalism in Section 2, we carry out numerical calculations in this section, taking snow and ice as an example of a random medium consisting of a collection of dielectric particles. For the integration involved, if only the integral value is concerned, we use the Gauss–Legendre quadrature method.

A. Absorption Efficiency

First, we calculate the integral value of Eqs. (7) by using Gaussian quadratures. Because the abscissas and weights of the n-point Gauss–Legendre quadrature formula are based on the interval $(-1, 1)$, we transform the actual integration interval into the $(-1, 1)$ range.[36] Comparison of the results with exact Mie computations[2] is shown in Figs. 3 and 4. The variation of the absorption efficiency Q_{abs} with particle size parameter $x = 2\pi a/\lambda$ for wavelength $\lambda = 0.5$ μm is shown in Fig. 3(a). The dashed curve is the absorption efficiency Q_{abs} calculated by the Mie code,[2] and the solid curve is that computed by the GOMsphere code. To assess the deviation of the GOM results from the Mie results, we define the percentage difference in the absorption efficiency as

$$\Delta_{\text{abs}} = \frac{Q_{\text{abs}}^{\text{Mie}} - Q_{\text{abs}}^{\text{Geo}}}{Q_{\text{abs}}^{\text{Mie}}} 100\%. \qquad (18)$$

The dependence of Δ_{abs} on x for $\lambda = 0.5$ μm is shown in Fig. 3(b). The average difference for size parameter x in the range from 10 to 10^4 is 1.46% owing to many extremely narrow peaks (ripple structure). If these peaks are ignored, the difference should be smaller.[11] For large particles with x from 5000 to 10,000, the average difference is 1.03%. As x increases, the difference decreases to zero. The variation of the absorption efficiency for a wavelength with larger absorption such as $\lambda = 2.0$ μm is shown in Fig. 4. The results for $\lambda = 2.0$ μm is obtained by using the same procedure as for $\lambda = 0.5$ μm. As the size parameter increases, Q_{abs} approaches an asymptotic value as indicated by results from both the Mie calculation and the GOM [Fig. 4(a)]. The results obtained by the GOM converge to the Mie results when the size parameter increases. The average Δ_{abs} versus x is shown in Fig. 4(b). From this figure it is readily seen that the deviation of the GOM from the Mie results approaches zero as $x > 4000$. Δ_{abs} decreases monotonically with size parameter when $x > 30$, with a maximum of Δ_{abs} occurring at $x \approx 30$. For $x \geq 220$, $\Delta_{\text{abs}} < 5\%$. For x values between 10 and 10,000, the average difference is 0.6%, and, for large particles with x from 5000 to 10,000, the average difference is 0.13%. For a composite snow grain as large as 1 cm, the size parameter can be as large as 100,000. GOMsphere works for any size parameter, whereas, for MIE0, $x < 20,000$. From Figs. 3 and 4 we can see that when $x > 300$, the difference is <4%; when $x > 1000$, the difference <0.7%. Therefore results for x values only up to 10,000 are shown in Figs. 3 and 4. In this paper the absorption efficiency Q_{abs} is calculated by using Eq. (7b), which does not include the above-edge and below-edge terms that account for the surface wave effect.[37,38] The surface wave effect plays a role only for small size parameters. It can be seen from Figs. 4 and 9 (see Subsection 3.B) that, when the size parameter exceeds a threshold, the difference between GOMsphere and
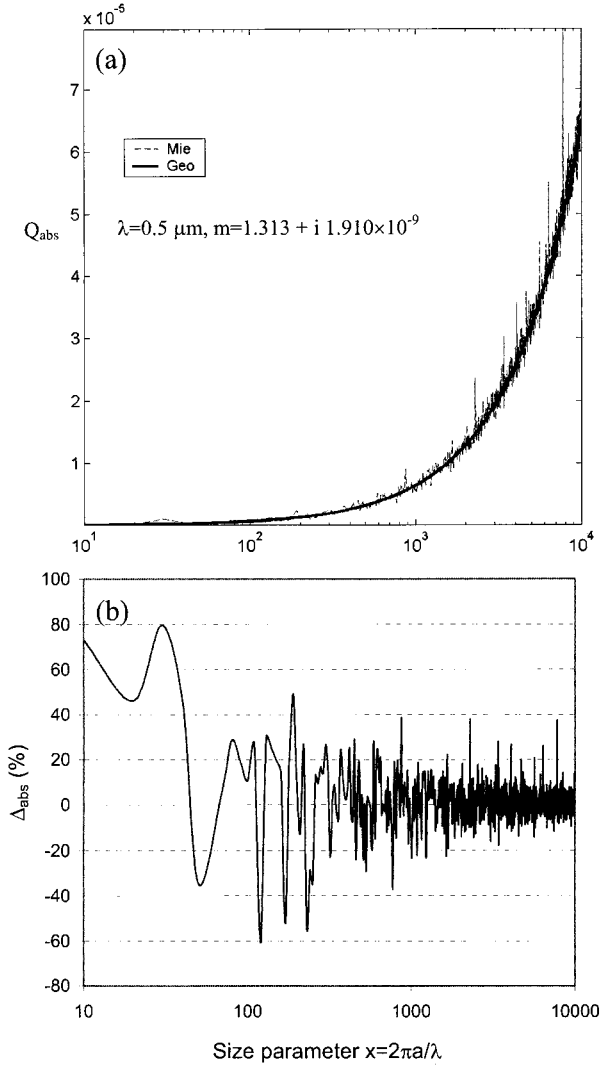
Fig. 3. (a) Absorption efficiency versus size parameter $x = 2\pi a/\lambda$ for wavelength $\lambda = 0.5$ μm corresponding to refractive index $m = 1.313 + i1.910 \times 10^{-9}$. The absorption efficiency is calculated using Mie scattering theory (dashed curve) and GOM (solid curve). (b) Percentage difference $\Delta_{abs} = [(Q_{abs}{}^{Mie} - Q_{abs}{}^{Geo})/Q_{abs}{}^{Mie}]100\%$ versus size parameter.
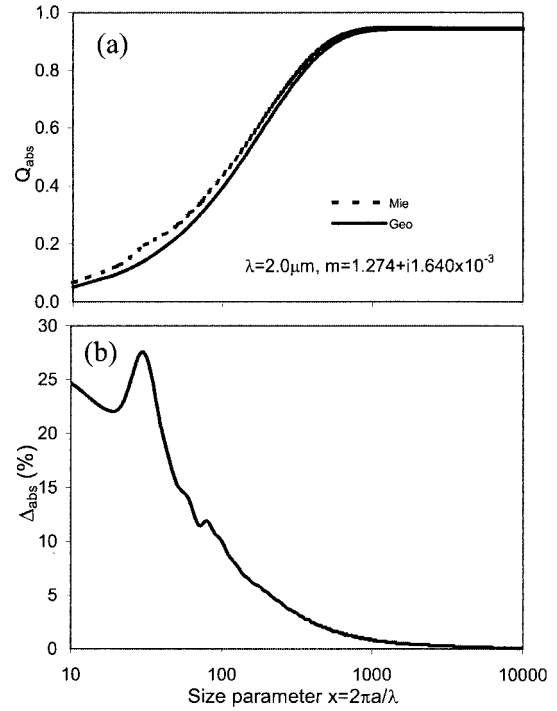

Fig. 4. (a) Absorption efficiency versus size parameter $x = 2\pi a/\lambda$ for wavelength $\lambda = 2.0$ μm corresponding to refractive index $m = 1.274 + i1.640 \times 10^{-3}$. Absorption efficiency is calculated by using the Mie scattering theory (dashed curve) and GOM (solid curve). (b) Percentage difference $\Delta_{abs} = [(Q_{abs}{}^{Mie} - Q_{abs}{}^{Geo})/Q_{abs}{}^{Mie}]100\%$ versus size parameter.

Mie calculations is negligible. Thus for large spheres, the effect of surface waves is negligible.

B. Scattering Efficiency and Phase Function

1. Near-Field Scattering

Using the same procedure as in Subsection 3.A, we may integrate Eq. (14b) numerically. For visible light, for instance, $\lambda = 0.5$ μm, $Q_{sca} \approx 1.0$ for any x because the absorption is very small (Fig. 3). In the near-infrared part of the spectrum, the scattering efficiency decreases with size parameter and approaches an asymptotic value. For instance, Fig. 5 shows the variation of the near-field scattering efficiency with the size parameter $x = 2\pi a/\lambda$ for the wavelength $\lambda = 2.0$ μm. The far-field scattering efficiency for $\lambda = 2.0$ μm (Subsection 3.B.2) is also included for comparison.

We can see that the difference between the far-field and the near-field scattering efficiencies is exclusively due to Fraunhofer diffraction.

The phase function Eq. (14a) and the asymmetry factor g can be written in the following forms when they are combined with Eq. (13):

$$P(\Theta) = \frac{2 \sum\limits_{j,\Theta_i} \sum\limits_p |\epsilon_p{}^j|^2 D(j, \Theta_i, \Theta)}{\int_0^\pi \sum\limits_{j,\Theta_i} (|\epsilon_\parallel{}^j|^2 + |\epsilon_\parallel{}^j|^2) D(j, \Theta_i, \Theta)\sin\Theta d\Theta},$$

(19a)

$$g = \frac{\int_0^\pi \sum\limits_{j,\Theta_i} \sum\limits_p |\epsilon_p{}^j|^2 D(j, \Theta_i, \Theta)\cos\Theta \sin\Theta d\Theta}{\int_0^\pi \sum\limits_{j,\Theta_i} (|\epsilon_\parallel{}^j|^2 + |\epsilon_\perp{}^j|^2) D(j, \Theta_i, \Theta)\sin\Theta d\Theta}.$$

(19b)

The angle of the emergent ray (scattering angle) at the jth interface from the sphere that deviates from the incident direction is[10,19,33]

$$\cos\Theta = \cos[2(j - 1)|\Theta_t| - 2\Theta_i - (j - 2)\pi]. \quad (20)$$

For a given scattering angle Θ, we need to find all the sets of (j, Θ_i) that satisfy Eq. (20), so that the right-

hand side of Eq. (20) can be evaluated. The method to obtain (j, Θ_i) is as follows. First, scan the j from 1 to N, and, for each j, solve Eq. (20) for all possible roots of Θ_i. Then substitute each set of (j, Θ_i) into Eqs. (19). Summing all the sets of (j, Θ_i) gives the phase function and the asymmetry factor.

To solve the intractable trigonometric equation (20), let us first transform it into a polynomial equation, which is easier to solve. Setting $S = \tan(\Theta_i/2) \in [0, 1]$, so that

$$\sin\Theta_i = \frac{2S}{1 + S^2}, \qquad \cos\Theta_i = \frac{1 - S^2}{1 + S^2},$$

Eq. (20) becomes

$$f(S) = \frac{(-1)^{j-2}}{(1 + S^2)^2}\{(1 - 6S^2 + S^4)\cos[2(j-1)|\Theta_t|]$$
$$+ 4S(1 - S^2)\sin[2(j-1)|\Theta_t|]\} - \cos\Theta$$
$$= 0, \qquad (21)$$

with

$$\Theta_t = \sin^{-1}\left(\frac{1}{\hat{m}}\frac{2S}{1 + S^2}\right)$$
$$= -i\,\ln\left\{i\,\frac{1}{\hat{m}}\frac{2S}{1 + S^2} + \left[1 - \left(\frac{1}{\hat{m}}\frac{2S}{1 + S^2}\right)^2\right]^{1/2}\right\}. \qquad (22)$$

In Eq. (21), complex refraction angle Θ_t is a function of S and thus is a dummy variable for the calculation of the phase function. Once the root S is found, by substituting S into Eq. (22), we can obtain the complex refraction angle Θ_t. For a given Θ, we can find values of Θ_i corresponding to different values of j (interface number) through the solution of Eq. (21), and then, by inserting Θ and Θ_i's into Eqs. (19), we obtain $P(\Theta)$. To find the roots (S) of Eq. (21) for a given scattering angle Θ, we adopt the following methods. First, we bracket the roots and then utilize a hybrid algorithm based on the bisection and the Newton–Raphson methods.[39] As the solution S is within $[0, 1]$, we calculate brackets for a maximum number of possible roots for n (= $n$max) distinct intervals, each of which contains at most one root for each interface. A trial-and-error method is used to find $n$max. The core procedure adopted to calculate the phase function for near-field scattering is shown in Fig. 6. Given the wavelength, the size (radius) of the sphere, and the scattering angle Θ, we scan the interface number j to obtain a reasonable large value $j$max (larger than the interface number, Subsection 2.A). For each interface, we search for all possible roots. Appropriate redirection is performed to include all possible sets of (j, Θ_i) in the calculation of the phase function and the asymmetry factor [Eqs. (19)]. The phase function versus scattering angle for near-field scattering is shown in Fig. 7 for a snow grain of 1-cm radius. The dark solid curve is for
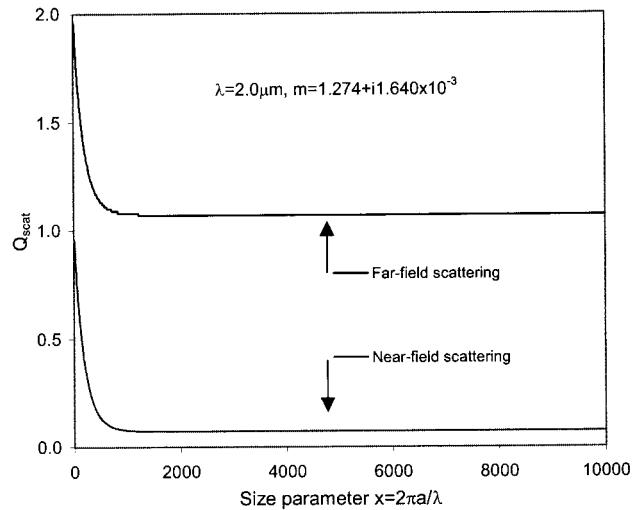

Fig. 5. Near-field scattering efficiency versus size parameter $x = 2\pi a/\lambda$ for wavelength $\lambda = 2.0$ μm. The far-field scattering efficiency for $\lambda = 2.0$ μm is also included for comparison. The tolerance number $\varsigma = 10^{-8}$. The difference between the far-field and the near-field scattering efficiencies is due only to Fraunhofer diffraction.

wavelength $\lambda = 0.5$ μm, and the light solid curve is for $\lambda = 2.0$ μm. For the visible-light channel, the rainbows appear at the angles where there are peaks. However, for the near-infrared channel, the transmitted energy is attenuated so quickly that almost no energy is available to reach the third interface where the primary rainbow is expected to appear. Thus the phase function for the near-infrared wavelength is much smoother than that for the visible wavelength. To compare the results from the GOMsphere code developed in this paper with those from a Monte Carlo code,[23] we show the phase function for refractive index $\hat{m} = 1.333 + i0.0$ in Fig. 8. The results obtained by the Monte Carlo code are taken from Table 1 of the paper by Kokhanovsky and Nakajima.[21] Figure 8 shows that the agreement between the two codes is remarkably good. The phase function calculated by using the GOMsphere code with $N = 2$ rather than with the truncation formula [Eq. (4)] is also shown in Fig. 8. For scattering angle $\Theta \leq 90°$, because the difference between the GOMsphere results using Eq. (4) and $N = 2$ is within 5%, the calculation with $N = 2$ gives very good results. But for $\Theta > 90°$, the phase function with $N = 2$ does not agree well with any of the GOMsphere results using the truncation formula and the Monte Carlo results. This corroborates the results by Glantschnig and Chen[33] that the geometrical-optics approximation for $N = 2$ agrees well with exact Mie calculations for incidence angles $\Theta_i \leq 60°$, whereas it does not for larger incidence angles. Phase functions calculated with $N = 2$ cannot intrinsically reproduce the rainbow peaks because the primary rainbow appears at the third interface,[32] but those calculated with the GOMsphere code using the truncation formula can
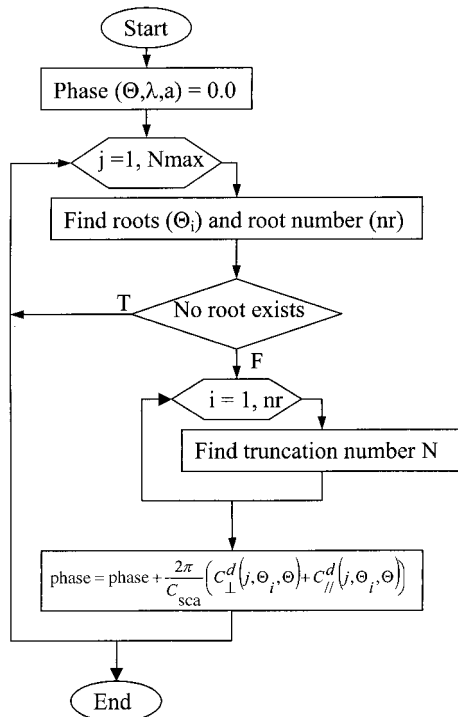
Fig. 6. Flow chart for the computational procedure adopted to compute the phase function for near-field scattering. T = true, F = false. The root finding is based on a combination of bracketing method and a hybrid algorithm based on the bisection and the Newton–Raphson methods. The truncation number is determined by Eq. (4).

exactly reproduce all the rainbow peaks predicted by analytical results.[10,19,32]

2. Far-Field Scattering

The scattering efficiency for the far-field scattering takes the form

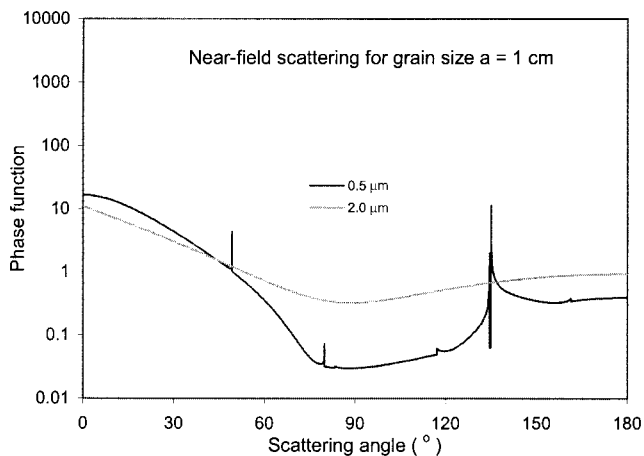$$Q_{\text{sca}}{}^F = Q_{\text{sca}}{}^N + 1. \qquad (23)$$

Fig. 7. Phase function for near-field scattering versus scattering angle Θ for a snow sphere of radius $a = 1$ cm for wavelength $\lambda = 0.5$ and 2.0 μm. Each peak in the visible curve corresponds to the position of a rainbow. The tolerance number $\varsigma = 10^{-8}$.
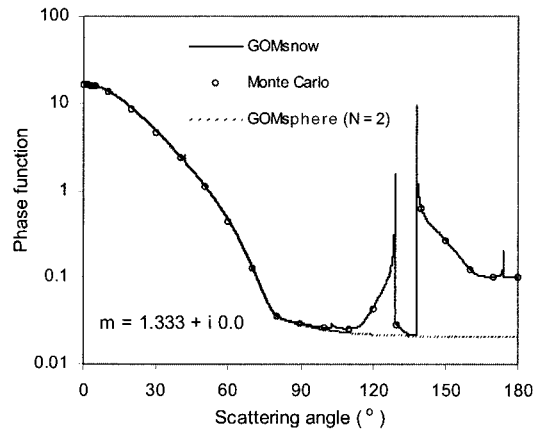

Fig. 8. Comparison of the phase function calculated with GOMsphere with that from a Monte Carlo code[21,23] for the nonabsorbing case of $\hat{m} = 1.333 + i0.0$. The tolerance number $\varsigma = 10^{-8}$. The phase function calculated by using $N = 2$ rather than by using the truncation formula [Eq. (4)] is also shown.

The phase function is the same as Eq. (17), and the asymmetry factor g is determined by Eq. (10). Following the same procedure as in Subsection 3.B.1 to find all the sets of (j, Θ_i) for a given scattering angle, we may evaluate the scattering efficiency, the asymmetry factor, and the phase function. For a dielectric sphere such as a snow grain, whose absorption of visible light is negligible, the scattering efficiency is approximately 2.0. For the near-infrared spectrum, for instance, $\lambda = 2.0$ μm, the absorption by snow is much larger than in the visible, and the scattering efficiency is well below 2.0. The dependence of Q_{scat} on the size parameter is shown in Fig. 9. When $x \geq 1300$, Q_{scat} is almost constant. To compare results from GOMsphere with those from Mie scattering computations, we show in Fig. 9(a) Q_{scat} versus size parameter x obtained from both GOM and Mie computations. The inset of Fig. 9(a) shows the results for x up to 10,000. The difference between the GOM and the Mie results is discernible only at small x values. Figure 9(b) shows the relative deviation between GOM and Mie computations. For $x \geq 110$, the relative deviation is smaller than 5%, and, for $x \geq 350$, it is smaller than 1%. When these deviations are considered with the comparisons at other wavelengths, we conclude that the scattering efficiency calculated by using GOMsphere agrees well with the Mie calculation for x larger than approximately 200.

Phase functions for far-field scattering are shown in Fig. 10. For comparison, the phase functions of the near-field scattering are also shown. Figure 10(a) is for $\lambda = 0.5$ μm, and Fig. 10(b) is for $\lambda = 2.0$ μm. For the same wavelength, the structures of the phase function for the near and far fields are similar, except in the forward direction in which there is strong forward scattering in the far field due to Fraunhofer diffraction. The difference between different wavelengths for far-field scattering is similar to that for the near-field scattering. For visible light, multiple rainbows appear, whereas in the near-

infrared region no rainbows are observed for the same reason as described in Subsection 3.B.1.

4. Discussion and Conclusions

A new geometrical-optics code, GOMsphere, has been developed to compute scattering and absorption cross sections of large dielectric particles of arbitrary complex refractive index on the basis of the truncation of the number of internal reflections and transmissions of a specific optical ray. Different GOM codes rely on different methods to control the run of the code. The present code uses the ratio of the energy flux incident at the jth interface (j is an integer) to that incident at the first interface ($j = 1$) as a control or criterion to determine the minimum number (truncation number) of internal reflections required for convergence. This truncation number N is a nonlinear function of the angle of incidence, increasing rapidly when the incidence angle is large. Comparison of the phase function calculated with GOMsphere that uses (i) a constant N (for example, $N = 2$) and (ii) a variable N [based on the truncation formula Eq. (4)] with that of a Monte Carlo code showed that $N = 2$ gives good results for scattering angles smaller than 90°, but it does not for larger scattering angles. Compared with the Monte Carlo results, the variable (incidence angle–dependent) N gives much better results than $N = 2$ because N must increase with the incidence angle to achieve a fixed truncation tolerance number. $N = 2$ intrinsically cannot reproduce the phase function structure with rainbow peaks. These results corroborate the findings by Glantschnig and Chen[33] that for $N = 2$ GOM results did not give good results when the incidence angle is greater than 60°. This new GOM code is applied to calculate the absorption efficiency, the scattering efficiency, and the scattering phase function for both near- and far-field scattering for large snow grains represented by homogeneous spheres. Comparison between results computed by the GOMsphere code and a Monte Carlo code[21,23] indicates that the agreement is good. Detailed scattering patterns can be constructed by using the GOMsphere code. Rainbow angles appearing in the phase function agree well with analytical results.[10,19,32] Owing to the difference in absorption or the imaginary part of the complex refractive index between the visible region and the near-infrared region of the solar spectrum, rainbows mainly appear in the visible, where absorption is so weak that there exists at least one internal reflection. Rainbows seldom appear in the near-infrared part of the spectrum, where absorption is large enough for the refracted portion of the energy to decrease to a negligible level without any internal reflection. For realistic cases, snow grains may not be homogeneous and spherical, and surface roughness may change the position and amplitude of the sharp rainbow peaks in the phase function. Phase function computations for both near- and far-field scattering show that the angular distribution of the light intensity scattered by large snow grains is more
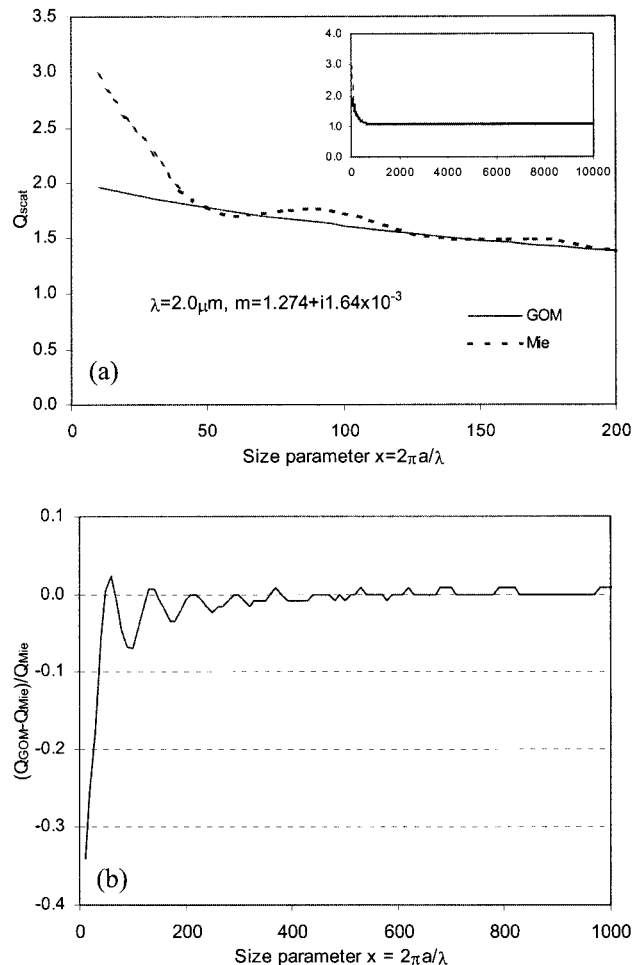

Fig. 9. (a) Far-field scattering efficiency versus size parameter $x = 2\pi a/\lambda$ for wavelength $\lambda = 2.0$ μm. In the inset the size parameter extends to 10,000. The difference between Mie and GOM calculations is very small except for small size parameters (<200). (b) The deviation of the scattering coefficient calculated by the GOMsphere code from that obtained by the MIE0 code. When $x \geq 110$, the deviation is smaller than 5%. For both (a) and (b) the truncation tolerance number $\varsigma = 10^{-8}$.

evenly distributed in the near infrared than in the visible.

Results computed by the GOMsphere code agree well with those computed by the MIE0 code[1,2] for size parameters $x \geq 200$ (difference $< 5\%$). GOMsphere is valid for any size parameter larger than 200, whereas the MIE0 code is valid for size parameters smaller than 20,000. Thus the GOMsphere and MIE0 codes can be combined to calculate single-scattering properties (single-scattering albedo and phase function) for any wavelength from the ultraviolet to the microwave and for arbitrary particle size. To maintain a definite accuracy, one should ensure that the size parameter is large enough (for instance, ≥ 300) when using GOMsphere. The computing time of the GOMsphere code is almost independent of the size parameter, whereas for the MIE0 code the size parameter is limited ($x < 20,000$) and the computing time is long when the size parameter is
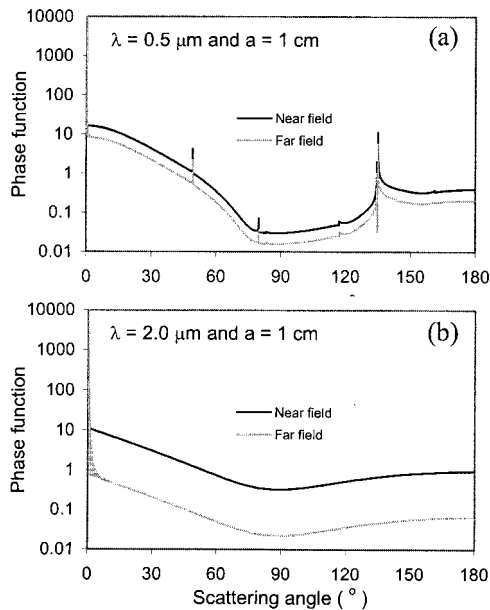
Fig. 10. Phase function for far-field scattering versus scattering angle Θ for a snow sphere of radius $a = 1$ cm for wavelength (a) $\lambda = 0.5$ μm and (b) $\lambda = 2.0$ μm. The truncation tolerance number $\varsigma = 10^{-8}$. For comparison, near-field results are also shown. Each peak in the visible curve corresponds to the position of a rainbow. Strong forward scattering due to Fraunhofer diffraction appears in the far-field scattering phase function.

large. The computation time of GOMsphere depends sensitively on the tolerance number. The larger the tolerance number, the faster the code. In the calculation of the phase function, the incidence angle is integrated over its whole range of values to obtain the phase function at each scattering angle. The GOMsphere code agrees well with a Monte Carlo code in the phase function calculation for all incidence and scattering angles (Fig. 8). Although the rainbow structure in the phase function produced by the GOM code agrees well with analytical results,[10,19,32] no glory peak at $\Theta = 180°$, as is expected from the Mie calculation, is observed in the phase function calculated by using the GOMsphere code.

The GOMsphere code is a computer program written in ANSI 77 standard FORTRAN to calculate the absorption coefficients, scattering coefficients, and phase function for both near- and far-field scattering of unpolarized radiation by large homogeneous dielectric spheres. For general-purpose applications, the input parameters required are the wavelength of the light in meters, the radius of the particle in meters, the particle refractive index, and the scattering angle in radians. If only absorption and scattering cross sections are needed, the scattering angle is irrelevant. The code and associated information can be downloaded from http://www.ees.nmt.edu/zhou/GOMsphere/.

References and Notes

1. W. J. Wiscombe, "Mie scattering calculations: advances in technique and fast, vector-speed computer codes," NCAR Tech. Note, NCAR/TN-140+STR (National Center for Atmospheric Research, Boulder, Colo., 1979).
2. W. J. Wiscombe, "Improved Mie scattering algorithms," Appl. Opt. **19,** 1505–1509 (1980).
3. Y.-X. Hu and K. Stamnes, "An accurate parameterization of the radiative properties of water clouds suitable for use in climate models," J. Clim. **6,** 728–742 (1993).
4. K.-N. Liou and Y. Takano, "Light scattering by nonspherical particles: remote sensing and climate implications," Atmos. Res. **31,** 271–298 (1994).
5. M. I. Mishchenko, "Calculation of the amplitude matrix for a nonspherical particle in a fixed orientation," Appl. Opt. **39,** 1026–1031 (2000).
6. F. M. Schulz, K. Stamnes, and J. J. Stamnes, "Scattering of electromagnetic waves by spheroidal particles: a novel approach exploiting the T matrix computed in spheroidal coordinates," Appl. Opt. **37,** 7875–7896 (1998).
7. H. A. Eide, J. J. Stamnes, K. Stamnes, and F. M. Schulz, "New method for computing expansion coefficients for spheroidal functions," J. Quant. Spectrosc. Radiat. Transfer **63,** 191–203 (1999).
8. P. Yang and K. N. Liou, "Geometric-optics-integral-equation method for light scattering by nonspherical ice crystals," Appl. Opt. **35,** 6568–6584 (1996).
9. S. C. Colbeck, "Grain clusters in wet snow," J. Colloid Interface Sci. **72,** 371–384 (1979).
10. H. C. van de Hulst, *Light Scattering by Small Particles* (Wiley, New York, 1957).
11. C. F. Bohren and D. R. Huffman, *Absorption and Scattering of Light by Small Particles* (Wiley, New York, 1983).
12. H. Bager, *Physics and Mechanics of Snow as a Material* (U. S. Army Cold Region Research and Engineering Laboratory, Hanover, N.H., 1962).
13. M. Sturm, K. Morris, and R. Massom, "The winter snow cover of the West Antarctic pack ice: its spatial and temporal variability," in *Antarctic Sea Ice: Physical Processes, Interactions and Variability*, M. O. Jeffries, ed., Vol. 74 of Antarctic Research Series (American Geophysical Union, Washington, D.C., 1998), pp. 1–18.
14. R. A. Massom, V. I. Lytle, A. P. Worby, and I. Allison, "Winter snow cover variability on East Antarctic sea ice," J. Geophys. Res. **103,** 24837–24855 (1998).
15. C. Haas, "The seasonal cycle of ERS scatterometer signatures over perennial Antarctic sea ice and associated surface ice properties and processes," Ann. Glaciol. **33,** 69–73 (2001).
16. K. Morris and M. O. Jeffries, "Seasonal contrasts in snow cover characteristics on Ross Sea ice floes," Ann. Glaciol. **33,** 61–68 (2001).
17. R. A. Massom, H. Eicken, C. Haas, M. O. Jeffries, M. R. Drinkwater, M. Sturm, A. P. Worby, X. Wu, V. I. Lytle, S. Ushio, K. Morris, P. A. Reid, S. G. Warren, and I. Allison, "Snow on Antarctic sea ice," Rev. Geophys. **39,** 413–445 (2001).
18. R. A. Massom, M. R. Drinkwater, and C. Haas, "Winter snow cover on sea ice in the Weddell Sea," J. Geophys. Res. **102,** 1101–1117 (1997).
19. X. Zhou, "Optical remote sensing of snow on sea ice: ground measurements, satellite data analysis, and radiative transfer modeling," (Ph.D. thesis, University of Alaska, Fairbanks, Alaska, 2002).
20. A. W. Nolin and J. Dozier, "A hyperspectral method for remotely sensing the grain size of snow," Remote Sens. Environ. **74,** 207–216 (2000).
21. A. A. Kokhanovsky and T. Y. Nakajima, "The dependence of phase functions of large transparent particles on their refractive index and shape," J. Phys. D **31,** 1329–1335 (1998).

22. H. M. Nussenzveig, *Diffraction Effects in Semiclassical Scattering* (Cambridge U. Press, London, 1992).

23. T. Y. Nakajima, T. Nakajima, and A. A. Kokhanovsky, "Radiative transfer through light-scattering media with nonspherical large particles: direct and inverse problems," in *Satellite Remote Sensing of Clouds and the Atmosphere II*, J. D. Haigh, ed., Proc. SPIE **3220,** 2–12 (1998).

24. D. J. Wielaard, M. I. Mishchenko, A. Macke, and B. E. Carlson, "Improved T-matrix computations for large, nonabsorbing and weakly absorbing nonspherical particles and comparison with geometrical-optics approximation," Appl. Opt. **36,** 4305–4313 (1997).

25. S. G. Warren, "Optical constants of ice from the ultraviolet to the microwave," Appl. Opt. **23,** 1206–1225 (1984). See Ref. 26 for the upgrade.

26. The updated compilation of the ice optical constant was done by B. Gao, W. Wiscombe, and S. Warren and is available by anonymous ftp to climate.gsfc.nasa.gov in the directory/pub/Wiscombe/Refrac_Index/ICE.

27. L. Kou, D. Labrie, and P. Chylek, "Refractive indices of water and ice in the 0.65- to 2.5-μm spectral range," Appl. Opt. **32,** 3531–3540 (1993).

28. D. K. Perovich and J. W. Govoni, "Absorption coefficients of ice from 250 to 400 nm," Geophys. Res. Lett. **18,** 1233–1235 (1991).

29. C. F. Bohren and B. R. Barkstrom, "Theory of the optical properties of snow," J. Geophys. Res. **79,** 4527–4535 (1974).

30. E. Hecht, *Optics*, 3rd ed. (Addison-Wesley Longman, Reading, Mass., 1998).

31. M. Born and E. Wolf, *Principles of Optics*, 6th ed. (Pergamon, Oxford, UK, 1980).

32. K. N. Liou and J. E. Hansen, "Intensity and polarization for single scattering by polydisperse spheres: a comparison of ray optics and Mie theory," J. Atmos. Sci. **28,** 995–1004 (1971).

33. W. J. Glantschnig and S.-H. Chen, "Light scattering from water droplets in the geometrical optics approximation," Appl. Opt. **20,** 2499–2509 (1981).

34. A. A. Kokhanovsky, *Optics of Light Scattering Media: Problems and Solutions* (Praxis, Chichester, UK, 1999).

35. G. E. Thomas and K. Stamnes, *Radiative Transfer in the Atmosphere and Ocean* (Cambridge U. Press, Cambridge, UK, 1999).

36. P. J. Davis and P. Rabinowitz, *Methods of Numerical Integration*, 2nd ed. (Academic, Orlando, Fla., 1984), pp. 481–483.

37. H. M. Nussenzveig and W. J. Wiscombe, "Efficiency factors in Mie scattering," Phys. Rev. Lett. **45,** 1490–1494 (1980).

38. E. P. Zege and A. A. Kokhanovsky, "Integral characteristics of light scattering by large spherical particles," Izv. Atmos. Ocean. Phys. **24,** 508–512 (1988).

39. W. H. Press, S. A. Teukolsky, W. T. Vetterling, and B. P. Flannery, *Numerical Recipes in C: the Art of Scientific Computing*, 2nd ed. (Cambridge U. Press, Cambridge, UK, 1992), pp. 350–354.